

Performances Analysis of GNSS NLOS Bias Correction in Urban Environment Using a 3D City Model and GNSS Simulator

Nabil Kbayer, and Mohamed Sahnoudi

Abstract—The well-known conventional Least Squares (LS) and Extended Kalman Filter (EKF) are ones of the most widely used algorithms in science and particularly in localization with GNSS measurements. However, these estimators are not optimal when the GNSS measurements become contaminated by non-Gaussian errors including multipath (MP) and non-line-of-sight (NLOS) biases. On the other hand, this kind of ranging measurements errors occurs generally in urban areas where GNSS-based positioning applications require more accuracy and reliability. In this paper, we use additional information of the environment consisting of bias prediction from a 3D model and a GNSS simulator to exploit constructively NLOS measurements. We use this 3D GNSS simulator to predict lower and upper bounds of these biases. Then, we integrate this information in the position estimation problem by considering these biases as additive error and exploiting the bounds to end-up with a constrained state estimation problem that we resolve with existing Constrained Least Squares (CLS) and Constrained EKF (CEFK) algorithms. Experimental results using real GPS signals in Down-Town Toulouse show that the proposed estimator is capable of improving the positioning accuracy compared to conventional algorithms. Theoretical conditions have been established to determine the acceptable bias prediction error allowing better positioning performance than conventional estimators. Tests are conducted then to validate these conditions and investigate the influence of the bias prediction error on the localization performance by proposing new accuracy metrics.

Index Terms—GNSS, Multipath and NLOS reception, Positioning in urban canyons, PR bias bounds characterization, 3D GNSS simulator, 3D city model.

I. INTRODUCTION

FREE accessibility and considerable progress of Global Navigation Satellites Systems (GNSS) during recent years have paved the way for providing more and more reliable geolocation solutions essential for a broad range of technologies [1].

Indeed, the steep increase of applications relying on geolocation especially in urban environments has fostered a growing trend towards the use of GNSS for positioning in these areas. However, this exponential progress of GNSS applications in

land navigation is not without major hurdles in its course of development. It is generally acknowledged that reliable GNSS positioning is not ensured in harsh environments (urban canyons, forested or mountainous areas with restrained sky visibility). These environments present significant challenges for satellites positioning which explains the gap between user requirements on one side and the existing technologies on the other side. The build-up urban setting engenders this GNSS performance degradation that prevents satellite positioning systems from reaching the required navigation performance in terms of accuracy, integrity and availability. Tall buildings and surrounding objects present in harsh environments block the direct line-of-sight (LOS) signal from many satellites which reduce satellite visibility and degrade the position availability. The remaining non-masked received signals are often contaminated with ranging errors and have all together a poor geometrical distribution which corrupts the position accuracy by several meters of error [2].

The density of various obstacles surrounding the GNSS receiver lead to receiving reflected and diffracted signals from buildings, walls, vehicles and other objects. Contrary to common perceptions, these contaminated signals may have high power especially if reflected by glass, metal or wet surfaces. This situation produces a bias on the pseudo-range (PR) measurements and consequently biases the position calculation. Refs [3] and [4] classifies the signals received in indirect paths into two separate types: Multipath (MP) signal if the signal is received through both direct and alternative paths (hence received via multiple paths) and Non-Line-Of-Sight (NLOS) signal if the signal is received only through reflections. This NLOS bias is a positive ranging error that may be potentially unlimited. Even though both the NLOS reception and multipath interference are often grouped together as multipath, they are actually separate phenomena that cause very different ranging errors [4]. Therefore, it is important to deal with these two phenomena separately although they usually arise together in urban areas. To date, several studies have attempted to deal with the multipath problem through receiver-based techniques such as narrow-correlators [5]–[7]. In fact, received multipath signals deteriorate the correlation function shape within the receiver, and this effect produces biased pseudorange measurements. This distortion of correlation pic, caused by multipath reception, is highlighted in reference [4]. Receiver-based signal processing techniques in [5]–[7] mitigate multipath by separating out the direct and reflected signals within the receiver. Unfortunately, NLOS reception

The authors would like to thank the French Space Agency (CNES) for funding this research project: SPRING Usage for Modeling Multipath Effects on a Receiver (SUMMER).

Nabil Kbayer is a PhD student at TésA Lab (7 Boulevard de la Gare, 31500 Toulouse) and ISAE-SUPAERO (French Institute of Aeronautics and Space), University of Toulouse, 31055 Toulouse, Cedex 4, France. His e-mail address is: nabil.kbayer@isae.fr.

Mohamed Sahnoudi is an Associate Professor at the French Institute of Aeronautics and Space (ISAE-SUPAERO), University of Toulouse, France (e-mail: mohamed.sahnoudi@isae.fr).

doesn't produce a distortion of the correlation pic as no direct signal is available. Then, these methods are not efficient in the case of NLOS reception since no direct signal is available. While some researches has been carried out on MP mitigation [5]–[9], there are still little solutions of the NLOS problem. In this paper, we investigate a novel robust GNSS solution that uses external bounds of PR biases to mitigate the effect of MP/NLOS phenomena in the state estimation towards a more accurate navigation.

This paper is divided into six main sections. In the second section, we propose a review of the state of the art of the use of 3D models for MP/NLOS mitigation. The third section illustrates the general GNSS problem statement and outlines the poor GNSS performance with results in an urban canyon environment in Toulouse (South-West of France). The novel robust estimator based on bias bounding is introduced in section 4 with simulation results using a 3D GNSS simulator. In section 5, we study the influence of PR errors and their correction on the positioning performance in terms of accuracy and we validate these theoretical results in section 6 by analyzing real data. Finally, some conclusions are summarized in section 7.

II. STATE-OF-THE-ART: GNSS POSITIONING IN PRESENCE OF MP/NLOS

One of the main drawbacks of the use of Global Navigation Satellites Systems (GNSS) for positioning in urban environments is the presence of ranging measurements errors combined with a low availability of signals and a poor geometrical satellite distribution due to satellite masking. In particular, signals contaminated by multipath interference and NLOS reception induce biased position estimation with several meters of PR errors in some harsh environments [10]. In order to achieve required accuracy in these environments, many researches had been conducted to overcome these challenges at the level of antenna design, hardware, receiver, post-receiver and in measurements or position domain [3], [11].

Broadly speaking, recent published studies on the field of GNSS positioning in harsh environments fall under three headings: LOS/NLOS distinction, i.e. NLOS detection and identification, MP/NLOS modeling and mitigation and MP/NLOS constructive use. The former tends to distinguish between clean LOS signals and NLOS range measurements. The literature on this category has highlighted several distinction criteria including using additional hardware for NLOS-LOS distinction, for instance dual polarization antenna [12], a GNSS antenna array and a sky-pointing camera [13]. Without using additional hardware, [3] argues for others simple indicators of NLOS reception such as elevation angle selection, C/N0-based NLOS detection and inter-satellite consistency checking [14]. Assuming that NLOS and LOS range estimates are perfectly distinguished, unhealthy measurements may be either discarded [15], down-weighted by robust estimation [16]–[18] or used constructively to enhance positioning performances [12]–[14].

The second approach tends to reduce the adverse impact of deteriorated MP/NLOS signals on the estimation accuracy.

Different configurations of antenna arrays are among the hardware solution for NLOS mitigation. Working in the receiver correlator output is another well-known approach. Most efficient technics represent standard features of professional grade GNSS receivers, in particularly those based on narrow and double-delta correlators [5], [6], [8], [9]. However, characterized by their high complexity, these in-receiver techniques are not effective in case of NLOS reception, because all of them are based on the assumption of LOS reception plus a reflected path [19]. Hence, NLOS mitigation can be performed on the data processing stage [11]. A number of other scientific studies carried out on NLOS elimination at the level of post-receiver, using robust estimation techniques [17], [18], MP modeling [20], [21] or by hybridizations with other external sensors [22].

Since at least four measurements are required for the position estimation, discarding faulty measurements may imply the unavailability of a PVT solution in some situations especially in deep urban canyons characterized by reduced visibility, i.e., a lack of measurements. Then, recent studies have focused on the constructive use of these MP/NLOS observables. One way of doing this is to predict the MP/NLOS bias via aiding information from a 3D city model and a propagation simulator and then correcting it in the PR measurements [22]–[24]. 3D models used jointly with a GNSS simulator characterize on-the-fly the measurements errors in urban environments and try to predict blockage and reflection of GNSS signals. With an initial position input, these models simulate the GNSS propagation in representative types of environments (e.g. open sky, urban and deep urban) and provide the user with several types of information such as the number and the characteristics of reflections, additional PR biases, etc. The quality and reliability of the simulated signals depend on how much close the a priori input position to the actual position to be estimated and on the reliability of the propagation modeling at the level of ray-tracing. Refs [23] and [24] have used the 3D model to predict PR errors and use it constructively on the estimation step. To manage the problem of the vicinity of the input point in the 3D simulator and the unknown position to be estimated, some studies use a grid of input points in the zone of interest which means considering signal reception at multiple candidate positions. The estimation of the position is then provided by comparison between the received observations at the receiver and ones of the information provided by the 3D model such as the sky visibility [2], [25], the delay information [26], the PR measurements [25], [27], [28] and the position consistency [3]. Others approaches combine a simplified 3D model of the environment with a probabilistic method to enhance performances [29], [30]. These techniques suppose that building layout is highly symmetric, which is mainly the case in the down-towns of most European cities. Using this simplified 3D model, called urban trench, path delays of MP/NLOS signals may be computed according to some assumed probabilities of reception.

The main challenge of using 3D models and simulators in the position estimation is the choice of the input position. An input point not sufficiently close to the unknown position to be estimated may induce erroneous ranging measurements.

Besides, although the 3D simulator are becoming more and more reliable, they contain a certain level of inaccuracy due to not modeling of the moving objects in the environment (cars, pedestrians...) and some immovable objects such as trees. In addition, it is obvious that the predicted biases from the 3D propagation model cannot be instantaneous and highly accurate especially with the sensitivity of the phase lag of the reflected signal. Therefore, we propose in this paper an original solution to handle this inaccuracy and this chicken and eggs problem of the input position choice. Instead of using directly the output bias value provided by the 3D simulator as it was classically done in previous studies, we will just use an upper and lower bound of these biases. We seek to study the problem of positioning with NLOS GNSS pseudorange (PR) in urban canyons by using a 3D city model and GNSS simulator to find the most appropriate bias bounds to constrain and correct then the PR measurements error. A novel sensitivity analysis on the influence of bias estimation on the localization accuracy using this method of PR measurements correction is proposed at the end of this study to validate the theoretical conditions presented in the fourth section.

III. GNSS PROBLEM FORMULATION

A. Problem Statement

A GNSS is a system allowing any user over the globe to locate upon a common referential, navigate and have a mean for synchronization on a common reference. The location estimation is ensured by a dedicated GNSS device able to estimate the time of arrival of signals along a line-of-sight (LOS) from at least four satellites. However, in general harsh areas, signals may be reflected by surfaces surrounding the GNSS receiver and then inducing an additional MP or NLOS bias in the ranging measurement. Then, the following linearized measurement equation formulates the GNSS problem [19]:

$$\mathbf{y} = \mathbf{H}_0 \mathbf{x} + \mathbf{b} + \mathbf{v} \quad (1)$$

Where, throughout this paper, the $[M, 1]$ state vector $\mathbf{x} = (x - x_0, y - y_0, z - z_0, b_c)^T$ contains the parameters of primary interest, i.e. the three coordinates of the user position $(x, y, z)^T$ and the receiver clock bias b_c , which is common between all the received satellites. $\mathbf{y} = (y_1, \dots, y_N)^T$ is the $[N, 1]$ linearised pseudorange (PR) measurements vector. \mathbf{H}_0 contains the unit line-of-sight (LOS) vectors between the satellites and the previous user position $\mathbf{x}_0 = (x_0, y_0, z_0)^T$. This matrix describes the linear connection between the measurements \mathbf{y} and the unknowns \mathbf{x} . $\mathbf{b} = (b_1, \dots, b_N)^T$ refers to the additional measurement bias caused by MP/NLOS receptions $[N, 1]$ and is commonly called PR bias. $\mathbf{v} = (v_1, \dots, v_N)^T$ is the measurement noise supposed to be a white Gaussian noise characterized by a known covariance matrix $\mathbf{R} = E[\mathbf{v}\mathbf{v}^T]$.

The cost function used to estimate \mathbf{x} is straightforward [31]:

$$\begin{aligned} J(\mathbf{y}|\mathbf{x}, \mathbf{b}) &= \|\mathbf{y} - \mathbf{H}_0 \mathbf{x} - \mathbf{b}\|_{\mathbf{R}^{-1}}^2 \\ &= (\mathbf{y} - \mathbf{H}_0 \mathbf{x} - \mathbf{b})^T \mathbf{R}^{-1} (\mathbf{y} - \mathbf{H}_0 \mathbf{x} - \mathbf{b}) \end{aligned} \quad (2)$$

Let us define the scalar product and norm related to the matrix \mathbf{R} as:

$$\forall \mathbf{a}, \mathbf{c} \in \mathbb{R}^N, \langle \mathbf{a}, \mathbf{c} \rangle_{\mathbf{R}^{-1}} = \mathbf{a}^T \mathbf{R}^{-1} \mathbf{c}, \quad \|\mathbf{a}\|_{\mathbf{R}^{-1}}^2 = \mathbf{a}^T \mathbf{R}^{-1} \mathbf{a} \quad (3)$$

We define the orthogonal projection on \mathbf{H}_0 with regard to this scalar product as:

$$\forall \mathbf{a} \in \mathbb{R}^N, \Pi_{\mathbf{R}^{-1}}^{\mathbf{H}_0} \mathbf{a} = \mathbf{H}_0 (\mathbf{H}_0^T \mathbf{R}^{-1} \mathbf{H}_0)^{-1} \mathbf{H}_0^T \mathbf{R}^{-1} \mathbf{a} \quad (4)$$

Let \mathbf{H}_0^\perp be the vector subspace orthogonal to \mathbf{H}_0 with regard to the scalar product (3). The orthogonal projection on this subspace is equal to:

$$\forall \mathbf{a} \in \mathbb{R}^N, \Pi_{\mathbf{R}^{-1}}^{\mathbf{H}_0^\perp} \mathbf{a} = \mathbf{a} - \Pi_{\mathbf{R}^{-1}}^{\mathbf{H}_0} \mathbf{a} = (\mathbf{I}_N - \Pi_{\mathbf{R}^{-1}}^{\mathbf{H}_0}) \mathbf{a} \quad (5)$$

Let us express now the cost function in (2):

$$J(\mathbf{y}|\mathbf{x}, \mathbf{b}) = \|(\Pi_{\mathbf{R}^{-1}}^{\mathbf{H}_0^\perp})(\mathbf{y} - \mathbf{b}) - \mathbf{H}_0 \mathbf{x}\|_{\mathbf{R}^{-1}}^2 + \|(\Pi_{\mathbf{R}^{-1}}^{\mathbf{H}_0})(\mathbf{y} - \mathbf{b})\|_{\mathbf{R}^{-1}}^2 \quad (6)$$

Using this last expression (6) as shown in Appendix A, we express the maximum likelihood (ML) state estimate as:

$$\hat{\mathbf{x}}_{ML} = \underset{\mathbf{x}}{\operatorname{argmin}} J(\mathbf{y}|\mathbf{x}, \mathbf{b}) = \mathbf{H}_0^+ (\mathbf{y} - \mathbf{b}) \quad (7)$$

where $\mathbf{H}_0^+ = (\mathbf{H}_0^T \mathbf{R}^{-1} \mathbf{H}_0)^{-1} \mathbf{H}_0^T \mathbf{R}^{-1}$ is the pseudo-inverse of \mathbf{H}_0 weighted by the inverse of the measurements covariance matrix \mathbf{R} . The error estimation in (7) is equal to:

$$\delta \mathbf{x}_{ML} = \hat{\mathbf{x}}_{ML} - \mathbf{x} = \mathbf{H}_0^+ \mathbf{v} \quad (8)$$

This ML estimator is the Minimum Variance Unbiased Estimator (MVUE) of problem (1) meaning that it is an unbiased estimator with the lowest variance, i.e. it minimizes the Mean Square Error (MSE) and hence maximizes the accuracy under the model Gaussianity assumption. As shown in Appendix A, the MSE of ML estimator is equal to:

$$\mathbf{MSE}[\hat{\mathbf{x}}_{ML}] = E[\delta \mathbf{x}_{ML} \delta \mathbf{x}_{ML}^T] = (\mathbf{H}_0^T \mathbf{R}^{-1} \mathbf{H}_0)^{-1} \quad (9)$$

This maximum likelihood estimator is equal to the least squares solution applied on the PR measurements corrected by MP-NLOS biases. Hence, it can be seen as a sum of a bias free-estimate computed as if no additional bias were present and a bias-correction term. Without having additional information on the MP-NLOS bias, the computation of this estimator will be impossible. In this case, a possible estimation of the state vector is given by the Least Squares (LS) solution:

$$\mathbf{x}_{LS} = \mathbf{H}_0^+ \mathbf{y} \quad (10)$$

The error of LS estimation is given by the following:

$$\delta \mathbf{x}_{LS} = \hat{\mathbf{x}}_{LS} - \mathbf{x} = \mathbf{H}_0^+ (\mathbf{b} + \mathbf{v}) \quad (11)$$

In the case of uncorrelated noise and MP-NLOS bias, based on the expression of LS estimation error in (11) as shown in Appendix A, the MSE of the LS estimator is equals to:

$$\mathbf{MSE}[\hat{\mathbf{x}}_{LS}] = E[\delta \mathbf{x}_{LS} \delta \mathbf{x}_{LS}^T] = (\mathbf{H}_0^T \mathbf{R}^{-1} \mathbf{H}_0)^{-1} + \mathbf{H}_0^+ E[\mathbf{b}\mathbf{b}^T] (\mathbf{H}_0^+)^T \quad (12)$$

The overall MSE (the trace of MSE matrix) of the LS estimator can be written as:

$$OMSE[\hat{\mathbf{x}}_{LS}] = \operatorname{Tr}\{(\mathbf{H}_0^T \mathbf{R}^{-1} \mathbf{H}_0)^{-1}\} + \operatorname{Tr}\{\mathbf{H}_0^+ E\{\mathbf{b}\mathbf{b}^T\} (\mathbf{H}_0^+)^T\} \quad (13)$$

This previous equation illustrates the effect of MP-NLOS biases on the positioning error. Indeed, using (9) and (13), without knowing PR bias, we show the following inequality:

$$OMSE[\hat{\mathbf{x}}_{LS}] \geq OMSE[\hat{\mathbf{x}}_{ML}] = \operatorname{Tr}\{(\mathbf{H}_0^T \mathbf{R}^{-1} \mathbf{H}_0)^{-1}\} \quad (14)$$

B. GNSS Positioning Performance in Urban Environments

Without having any additional information on the MP and NLOS measurement bias, the LS state estimate will not be accurate in the sense of minimizing the Mean Square Error (MSE). This performance degradation becomes more important in the presence of high ranging measurements errors caused by MP/NLOS phenomena in deep urban environments. In this section, we illustrate this aspect by evaluating the GNSS positioning accuracy in an urban environment in Toulouse.

1) General Experimental Setup:

Experiments have been carried out in Toulouse to assess the level of performance of GNSS positioning in harsh areas. The used GPS L1 C/A code PR measurements were recorded along the Capitole Square in Toulouse using an AsteRx3 SEPTENTRIO receiver and a SPAN Novatel system including a DGPS receiver tightly integrated with an IMU-FSAS (from iMAR), with decimeter level of accuracy. We consider the trajectory provided by the Novatel receiver as the reference trajectory. The measurement was sampled at 10 Hz.

For this test, we use a 4-min trajectory along a deep urban environment characterized by narrow streets and buildings alongside the streets. The following table summarizes the set of some of the received GPS/GLONASS signals during this measurement campaign.

TABLE I: SOME RECEIVED SIGNALS IN THE CONSIDERED URBAN SECTION (G FOR GPS SATELLITES AND R FOR GLONASS SATELLITES)

	G13	G15	G22	G28	R08	R09	R11
Elevation (°)	52.4	82.2	5.9	26	62	35	25.5
C/N0(dB-Hz)	42	47.7	35.5	27.7	34	24	28

The Sky-plot of the received GPS and GLONASS satellites in the tested deep urban section is shown in Fig. 1.

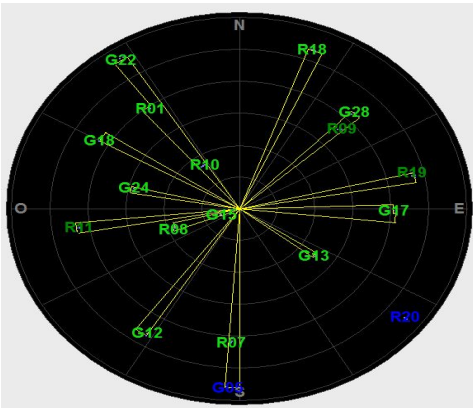


Fig. 1: Sky-plot of GPS/GLONASS satellites

2) Evaluation of GNSS Positioning in Urban Environments:

These recorded PR measurements collected along this urban canyon environment show how poor is the GNSS positioning performance in presence of MP and NLOS biases. The obtained results are shown in Fig. 2. This figure presents also the cumulative distribution function (CDF) of the trajectory position error with respect to the reference trajectory in each

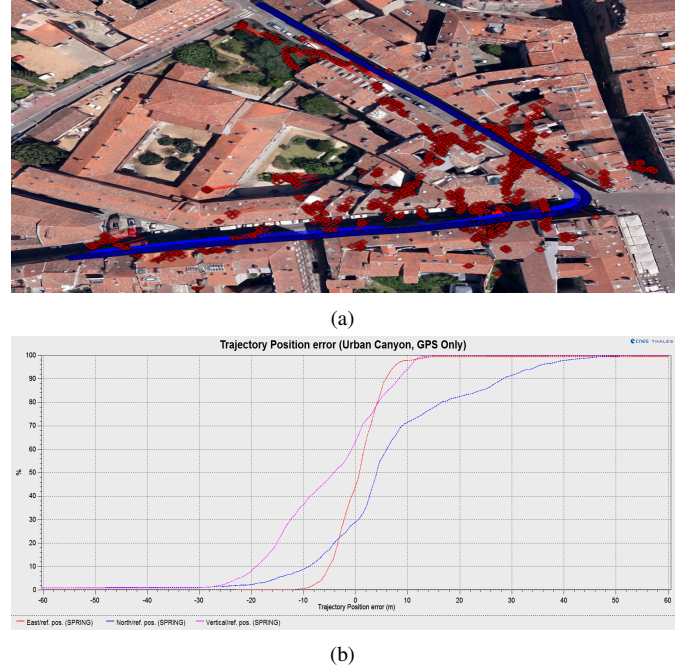


Fig. 2: Example vehicular results in Toulouse: 2(a) Positioning using Least Squares solution: Blue dots refer to the reference trajectory; red dots refer to the LS trajectory; 2(b) Localization errors distribution of the Least Squares solution: North, East and Vertical positioning errors in urban environments.

ENU direction using a conventional least squares with GPS signal only.

As shown in Fig. 2, it's obvious that GPS-based localization using conventional estimators in urban areas can be highly inaccurate. Satellite Shadowing, high Dilution Of Precision (DOP) and reception of signals contaminated by MP and NLOS biases are the main reasons of this degraded GNSS positioning. It is apparent from these curves that GNSS-based positioning accuracy is degraded since we obtain, for example, more than 10 meters of position error in the north direction in almost 40% of the time. Hence in this case, this status of technology doesn't match the user need in a wide range of application.

This poor GNSS localization performance stems from large ranging measurement errors and an unfavorable satellite geometrical distribution. Indeed, satellite masking and shadowing induce a bad satellite geometry which lead to a high DOP that exceed 1 in 100% of the samples in this scenario for both HDOP and VDOP. The mean value for both HDOP and VDOP are also high (4.2 for instance for HDOP in this case). Another interesting aspect that might be highlighted for GNSS-based localization is signal unavailability due to satellite masking by high buildings. We note that during an interesting part of the trajectory, there is a problem of satellite visibility, with less than four measurements available in some cases.

It is also worth noting that this poor GNSS localization performance in urban areas does not depends on the GNSS constellations or signals used. As explained in the introduction, it is clear that any GNSS signal may be reflected by building, walls or surfaces presents in the environment regardless the satellite constellation used. Although the multi-constellation aspect is essential in harsh environment settings to improve

signals availability, no enhancement is acquired in terms of ranging accuracy which is limited by physical phenomena of signal propagation. Then, the trajectory obtained using a conventional least squares with GPS and GLONASS signals is surely more accurate than the one obtained using only GPS signals but it does not reach the required navigation accuracy needed for most of GNSS-based applications in urban environments. Fig. 3 shows histograms of positioning errors in each ENU direction using conventional LS with GPS and GLONASS signals.

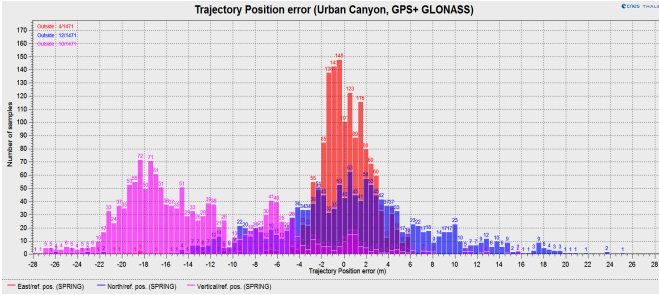


Fig. 3: Localization performance along an urban trajectory: North, East and Vertical positioning errors in bi-constellation mode

C. GNSS Pseudorange Correction

In this sub-section, we suppose that we can obtain an estimation of the PR bias using an external information source such as 3D GNSS simulator for instance. This estimation is referred to as \mathbf{c} . Also, we suppose that we build a new weighting matrix \mathbf{R}_b based on this predicted PR bias \mathbf{c} .

The final solution of problem (1) with measurement correction would be a corrected least squares (CLS) using the estimation of the PR bias and is expressed as:

$$\mathbf{x}_{CLS} = \mathbf{H}_b^+ \mathbf{y} \quad (15)$$

Where $\mathbf{y}_c = \mathbf{y} - \mathbf{c}$ are the corrected PR measurement and $\mathbf{H}_b^+ = (\mathbf{H}_0^T \mathbf{R}_b^{-1} \mathbf{H}_0)^{-1} \mathbf{H}_0^T \mathbf{R}_b^{-1}$ is the pseudo-inverse of \mathbf{H}_0 weighted by the inverse of the measurements covariance matrix \mathbf{R}_b that might be different from \mathbf{R} . The error of estimation is given by:

$$\delta \mathbf{x}_{CLS} = \hat{\mathbf{x}}_{CLS} - \mathbf{x} = \mathbf{H}_b^+ (\mathbf{b} + \mathbf{v} - \mathbf{c}) \quad (16)$$

If we note $\delta \mathbf{b} = \mathbf{b} - \mathbf{c}$ the error in the PR bias prediction, the accuracy of the CLS estimator is characterized by the **MSE**. Using straightforward matrices rules similar to those shown in Appendix A, we express the MSE of the CLS estimator as:

$$\begin{aligned} \mathbf{MSE}[\hat{\mathbf{x}}_{CLS}] &= E[\delta \mathbf{x}_{CLS} \delta \mathbf{x}_{CLS}^T] \\ &= (\mathbf{H}_0^T \mathbf{R}_b^{-1} \mathbf{H}_0)^{-1} + \mathbf{H}_b^+ E[\delta \mathbf{b} \delta \mathbf{b}^T] (\mathbf{H}_b^+)^T \end{aligned} \quad (17)$$

The overall **MSE** of the CLS estimator can be written as:

$$OMSE[\hat{\mathbf{x}}_{CLS}] = \text{Tr}\{(\mathbf{H}_0^T \mathbf{R}_b^{-1} \mathbf{H}_0)^{-1}\} + \text{Tr}\{\mathbf{H}_b^+ E[\delta \mathbf{b} \delta \mathbf{b}^T] (\mathbf{H}_b^+)^T\} \quad (18)$$

Because the weighting matrix \mathbf{R}_b is generally an augmented matrix version of the covariance \mathbf{R} , i.e. $\text{Tr}\{(\mathbf{H}_0^T \mathbf{R}_b^{-1} \mathbf{H}_0)^{-1}\} \geq \text{Tr}\{(\mathbf{H}_0^T \mathbf{R}^{-1} \mathbf{H}_0)^{-1}\}$ and because of

the presence of PR bias prediction error $\delta \mathbf{b}$ in expression (18), this yields the following inequality:

$$OMSE[\hat{\mathbf{x}}_{CLS}] \geq \text{Tr}\{(\mathbf{H}_0^T \mathbf{R}^{-1} \mathbf{H}_0)^{-1}\} = OMSE[\hat{\mathbf{x}}_{ML}] \quad (19)$$

This means that the conventional LS estimator doesn't reach the optimal **MSE** while the proposed CLS estimator does under the condition of low bias prediction error $\delta \mathbf{b}$. But, the accuracy of the proposed algorithm depends on the PR bias estimation used to correct the PR measurements. Hence, a good estimated PR bias that enhances performance compared to conventional methods must follow as much as possible the true bias as expressed in (18). In the following sub-section, we propose to use bias bounds estimated from a 3D GNSS simulator to both constrain and correct PR measurements.

IV. GNSS MEASUREMENT CORRECTION BY BIAS BOUNDING

A. Measurements correction using PR bias bounds

We evaluate the added-value of PR bias correction in term of localization performance along the deep urban path. To do that, we use our proposed algorithm in [32].

We assume that at every time step the MP-NLOS bias \mathbf{b} is bounded, i.e. we assume the following inequality for each time step and for each received PR signal:

$$(\mathbf{l})_n \leq (\mathbf{b})_n \leq (\mathbf{u})_n, \forall n = 1, 2, \dots, N$$

Where $\mathbf{l} = (\mathbf{l}_1, \dots, \mathbf{l}_N)^T$ refers to the lower bound of the PR bias and $\mathbf{u} = (\mathbf{u}_1, \dots, \mathbf{u}_N)^T$ is the upper bound of the PR bias. This bias bounding allows constraining the LOS measurement vector $\mathbf{H}_0 \mathbf{x}$:

$$\mathbf{c}_{inf} \leq \mathbf{H}_0 \mathbf{x} \leq \mathbf{c}_{sup} \quad (20)$$

Where $\mathbf{c}_{inf} = (\mathbf{y}_1 - \mathbf{u}_1 - 3\sigma_1, \dots, \mathbf{y}_N - \mathbf{u}_N - 3\sigma_N)^T$ is the lower bound of the LOS measurement vector $\mathbf{H}_0 \mathbf{x}$ and $\mathbf{c}_{sup} = (\mathbf{y}_1 - \mathbf{l}_1 + 3\sigma_1, \dots, \mathbf{y}_N - \mathbf{l}_N + 3\sigma_N)^T$ is the upper bound of the LOS PR vector $\mathbf{H}_0 \mathbf{x}$ and $\sigma_i^2 = \mathbf{R}_{i,i}, \forall i = [1, \dots, N]$.

Assuming that the bias is Gaussian between these two bounds and since the MP-NLOS bias and the measurement noise are independent, the total noise $\mathbf{b} + \mathbf{v}$ will have a non-zero Gaussian distribution with a covariance matrix equal to:

$$\mathbf{R}_b = \mathbf{R} + \text{diag}\{[(\mathbf{u}_n - \mathbf{l}_n)/6]^2\}_{n=1, \dots, N} \quad (21)$$

The mean value of the total noise distribution must be subtracted from the PR measurement vector when estimating the state vector. We get finally a constrained state estimate with PR measurements correction using PR bias bounds:

$$\begin{cases} \hat{\mathbf{x}}_{CLS} = \underset{\mathbf{x}}{\text{argmin}} \|\mathbf{y} - (\mathbf{u} + \mathbf{l})/2 - \mathbf{H}_0 \mathbf{x}\|_{\mathbf{R}_b^{-1}} \\ \mathbf{c}_{inf} \leq \mathbf{H}_0 \hat{\mathbf{x}}_{CLS} \leq \mathbf{c}_{sup} \end{cases} \quad (22)$$

This quadratic problem can be resolved using the Matlab routine `quadprog`. The obtained solution from (22) is referred to as the constrained solution and can be combined with a motion model to end-up with a constrained EKF with bias bounding, called CEKF. The proposed approach is summarized in the algorithm 1 below.

Algorithm 1 : Constrained LS with bias bounding (CLS)**Inputs:** \mathbf{y}, \mathbf{H}_0 **Output:** $\hat{\mathbf{x}}_{CLS}$

- 1: **Search area and grid of candidate positions:**
Define input points $\Gamma = \{\mathbf{x}_i = (x_i, y_i, z)^T\}$ where z is given by the 3D GNSS simulator.
- 2: **Bank of 3D PR bias measurements:**
Predict a bank of PR bias using SPRING, i.e. predict $\Omega = \{\mathbf{b}_{3D}(\mathbf{x}_i) = (\mathbf{b}_{3D}(\mathbf{x}_i)_1, \dots, \mathbf{b}_{3D}(\mathbf{x}_i)_N)^T\}$ for each input position and each received satellite.
- 3: **Lower and upper PR bias bounds:**
Define lower and upper bias bounds as:
 $\mathbf{l} = \min_{\mathbf{x}_i \in \Gamma} (\mathbf{b}_{3D}(\mathbf{x}_i)), \quad \mathbf{u} = \max_{\mathbf{x}_i \in \Gamma} (\mathbf{b}_{3D}(\mathbf{x}_i)).$
- 4: **Lower and upper bounds of LOS measurement $\mathbf{H}_0\mathbf{x}$:**
Compute $\mathbf{c}_{inf} = \mathbf{y} - \mathbf{u} - 3(\sigma)_{i=[1, \dots, N]}$ the lower bound, $\mathbf{c}_{sup} = \mathbf{y} - \mathbf{l} + 3(\sigma)_{i=[1, \dots, N]}$ the upper bound and $\mathbf{R}_b = \mathbf{R} + \text{diag}\{[(\mathbf{u}_n - \mathbf{l}_n)/6]^2\}_{n=1, \dots, N}$.
- 5: **Final Estimate:** LS applied to corrected PR with augmented covariance noise matrix and LOS PR bounding:

$$\left\{ \begin{array}{l} \hat{\mathbf{x}}_{CLS} = \underset{\mathbf{x}}{\text{argmin}} \|\mathbf{y} - (\mathbf{u} + \mathbf{l})/2 - \mathbf{H}_0\mathbf{x}\|_{\mathbf{R}_b^{-1}} \\ \mathbf{c}_{inf} \leq \mathbf{H}_0\hat{\mathbf{x}}_{CLS} \leq \mathbf{c}_{sup} \end{array} \right.$$

Ref [4] explains that NLOS reception and multipath interference are separate phenomena that exhibit different ranging errors. However, our proposed positioning algorithm is correcting the additional bias on PR measurements, based on PR bias bounds, without doing any distinction between different reception status of the GNSS signal (MP or NLOS reception). Hence, we have chosen to merge both MP and NLOS phenomena in this paper. The idea is to correct the additional pseudorange path, i.e. PR bias, in both cases of MP and NLOS receptions.

The performance of this algorithm will be evaluated in next sub-sections using bias bounds predicted with a reference system and bias bounds predicted using a 3D GNSS simulator.

B. Measurements correction with reference PR bias bounds

In this sub-section, we have used the same data recorded in an urban canyon environment with narrow streets and high buildings in down-town Toulouse displayed in the Fig. 2.

We first use artificial PR bias bounds based on true bias prediction. The prediction of the true PR bias is performed using the algorithm proposed in [33]. This algorithm is based on exploiting the errors in solutions or computed positions, i.e. positioning errors $\delta\mathbf{x}_{LS}$, to predict the errors in observations or PR measurements, i.e. PR bias \mathbf{b} . As expressed in (11), the positioning error of LS estimation $\delta\mathbf{x}_{LS}$ depends linearly on the pseudorange error \mathbf{b} . Hence, PR bias can be determined by simply inverting this equation as presented in [33]. To better illustrate this method, the main steps are summarized in algorithm 2.

PR bias represents the difference between the signal received through reflections, with or without reception of direct

Algorithm 2 : True PR bias prediction**Inputs:** \mathbf{y}, \mathbf{H}_0 **Output:** True bias prediction \mathbf{b}_{True}

- 1: **Reference satellite (most reliable satellite) selection:**
based on elevation criterion for example.
- 2: **True positioning error determination based on reference position:**
Compute $\delta\mathbf{x}_{LS} = \hat{\mathbf{x}}_{LS} - \mathbf{x}_{True}$, where \mathbf{x}_{True} is obtained from a reference system.
- 3: **Predict true PR bias:**
Using reference satellite and knowing the true positioning error, invert equation (11), i.e. $\delta\mathbf{x}_{LS} = \mathbf{H}_0^+(\mathbf{b} + \mathbf{v})$, to predict the PR bias term $(\mathbf{b} + \mathbf{v})$.

signal, and the direct LOS signal from the satellite. Position errors represent the difference between the estimated position using the least squares (LS) algorithm and the reference position. This error can be accurately estimated using the reference information of vehicle position provided by a DGPS receiver tightly integrated with an IMU.

As having a reference pseudorange, i.e. the value of direct line-of-sight signal, is difficult to obtain, the pseudorange error can be calculated using the error in the LS estimation. The main problem is having a reference of the receiver clock bias to apply this algorithm.

The receiver clock bias is eliminated by proceeding to a differentiation of all ranging measurements across satellites using a reference satellite. The selection of reference satellite is quite important. This satellite must have a reliable and almost clean ranging measurement. Basic indicators for this selection process include elevation angle and C/N0 values. Ref. [33] proposes a reference satellite selection using LOS probability obtained via signal power distributions using experimental data. In this work, we have used the elevation angle as an indicator for reference satellite selection.

In summary, this pseudorange bias prediction technique relies on the use of position errors using a reference system and the compensation of the clock bias using a reference satellite. This technique has been tested and validated using real GNSS data collected in Toulouse.

Based on this predicted true PR bias, we define upper and lower bias bounds for each received PR signal as:

$$\left\{ \begin{array}{l} \mathbf{l} = \mathbf{b}_{True} - \mathbf{m}, \quad \mathbf{m} \sim \mathcal{N}(\mu_{\mathbf{m}}, \sigma_{\mathbf{m}}^2) + m \\ \mathbf{u} = \mathbf{b}_{True} + \mathbf{M}, \quad \mathbf{M} \sim \mathcal{N}(\mu_{\mathbf{M}}, \sigma_{\mathbf{M}}^2) + M \end{array} \right. \quad (23)$$

Where \mathbf{b}_{True} is the true PR bias vector. In this sub-section, we have taken these constants equal to: $m = 17$ meters, $M = 12$ meters, $(\mu_{\mathbf{M}})_n \sim \mathcal{U}(0, 9)$, $(\mu_{\mathbf{m}})_n \sim \mathcal{U}(0, 6)$, $(\sigma_{\mathbf{M}})_n \sim \mathcal{U}(0, 5)$ and $(\sigma_{\mathbf{m}})_n \sim \mathcal{U}(0, 3)$, $\forall i = [1, \dots, N]$.

These used values of \mathbf{m} and \mathbf{M} are fixed as a way of illustration to assess the performance of the proposed positioning algorithm based on artificial PR bias bounds. These variables \mathbf{m} and \mathbf{M} are defined to make sure that the upper and lower bounds are the most variable possible from the predicted true

PR bias, with a Gaussian variation. Others values of m and M have been tested and give the same result.

By way of illustration, Fig. 4 shows these artificial bias bounds for PRN 28:

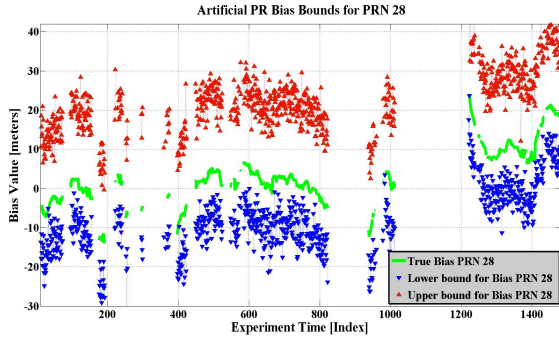


Fig. 4: Artificial Bias Bounds and True bias for satellite PRN 28: Artificial bias bounds are obtained using reference system

The accuracy of the position estimation depends essentially on the correction made by mean bias bounds. Curves of the trajectories obtained using conventional EKF (in red) and the CEKF estimator with bias correction (in green) is shown in Fig. 5(a). We illustrate also the uncertainty on the position estimation for each estimator by drawing the ellipsoidal confidence domain. The blue trajectory represents the reference trajectory obtained with the SPAN Novatel system.

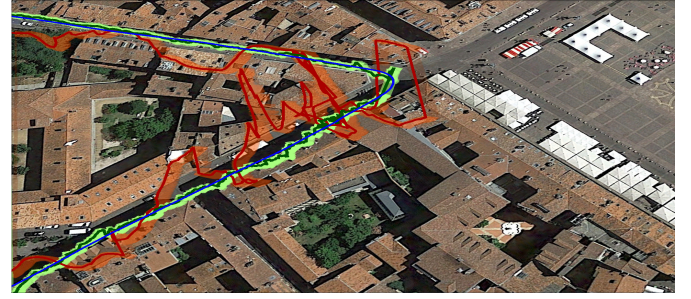
In Fig. 5(b), we have studied the positioning in a particular point in this urban trajectory. We display the reference point in blue dots, the CEKF solution and the conventional EKF position. The LOS paths are also displayed from the received satellites to the reference point. In this situation, only four signals are received of which two are in direct paths plotted in green. The other two signals, drawn in cyan, are received in NLOS situation. This figure shows that the CEKF solution gives better positioning performance compared to the conventional EKF solution in this case of reception of only four PR measurements: two LOS signals and two NLOS signals.

It can be clearly seen from Fig. 5 that the corrected EKF with bias bounding gives good positioning performance. Fig. 6 shows the cumulative distribution function of the horizontal position errors of EKF estimator, CLS with bias bounding and the CEKF with bias bounding. It is apparent from the CDF figure that our approach gives more positioning performance compared to the conventional EKF since we have less than 8 meters of horizontal positioning error in 99% of cases in this kind of harsh areas.

C. 3D GNSS simulator SPRING

SPRING is a GNSS simulator developed by the French Space Agency (CNES) that has the capability of simulating, via ray-tracing techniques, all paths to be received in a certain input position at a certain time.

3D GNSS simulator SPRING allows the simulation of the propagation of the GNSS signals inside a realistic 3D scene for an in depth analysis of the signal reception status. A ray tracing method is integrated to simulate the GNSS signal propagation in a representative and accurate model of the



(a)



(b)

Fig. 5: Positioning performance in urban canyons: 5(a) Example vehicular results in Toulouse; 5(b) An example of GNSS in presence of NLOS situation.

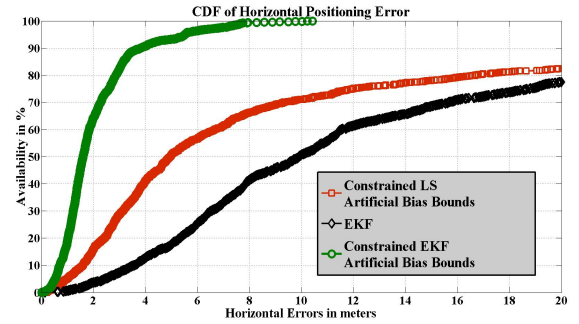


Fig. 6: CDF of horizontal errors using artificial bias bounds

3D scene. This propagation model, based on launching of rays for each possible direction starting from the receiving antenna, takes into account all types of propagations: free-space propagation, reflection, refraction, diffraction etc. Finally, a reception channel model and a receiver model enable the acquisition and tracking of the GNSS signals in order to calculate pseudoranges, phase and Doppler measurements of the acquired satellites.

The main steps used for 3D PR bias estimation at each candidate position are summarized in algorithm 3. It must be emphasised that PR receiver bias is omitted in 3D simulation as the receiver is supposed to be synchronized with emitted satellites.

D. GNSS Measurements correction by bias bounding using a 3D GNSS simulator

We use now the 3D GNSS simulator SPRING to define upper and lower bias bounds as explained in [32]. Tests were carried out to assess the level of performance achieved by PR measurement correction based on bias correction using bounds

Algorithm 3 : 3D GNSS Simulation using SPRING

Inputs: GPS Time, Satellite ephemeris, 3D city Model and input position \mathbf{x}_i

Output: 3D bias $\mathbf{b}_{3D}(\mathbf{x}_i)$

- 1: **Compute satellite positions** $\mathbf{x}_i^{Sat_i}$
 - 2: **Determine LOS distance between each satellite and the input position:**
For each satellite Sat_i , compute $PR_i^{LOS} = \|\mathbf{x}_i - \mathbf{x}_i^{Sat_i}\|_2$.
 - 3: **Predict 3D received PR measurements:**
For each satellite Sat_i , predict PR_i^{3D} , using the 3D model, ray-tracing algorithm and the receiver model implemented in SPRING.
 - 4: **Compute PR bias:**
As all the other ranging errors are not modelled, PR bias is the difference between predicted PR measurements and LOS distance: $[\mathbf{b}_{3D}(\mathbf{x}_i)]_i = PR_i^{3D} - PR_i^{LOS}$.
-

prediction from the 3D GNSS simulator SPRING [34]. We use now a 3D GNSS simulator to predict upper and lower bias bounds. We have used the same data recorded in the same urban canyon environment studied in the previous example above. For PR bias bounds prediction, we have used the algorithm described in [32] with a grid of 3×3 points centred in the true position and spaced by $(10^{-5})^\circ$ in longitude and latitude, i.e. 1 meter in north and east directions. After the PR bias bounds estimation using this grid, the CEKF position can be computed and compared to the conventional EKF position. Performances will depend on the quality of the PR bias bounds prediction using the 3D GNSS simulator.

As a way of illustration, the variation of the bias bounds using the 3D simulator SPRING is drawn in Fig. 7(a) for PRN 28 for example. Fig. 7(b) provides the CDF of horizontal positioning errors of both solutions.

The predicted PR bias bounds have a different variation compared to the true PR bias which means that the 3D estimated mean bias bounds have a higher variation than the true unknown PR bias variation. The previous CDF figure shows that the CEKF estimator gives a performance improvement compared to EKF with bias bounds estimated using a 3D GNSS simulator especially for high positioning errors.

Taken into account that the 3D simulator SPRING is under permanent improvement and evolution by CNES, these results shows the usefulness and the potential of these tools for positioning enhancement in presence in MP/NLOS biases.

The proposed method based on PR bias bounds is essentially sensitive to these PR bias correction by mean bias bounds and then to the bias bounds prediction as shown before. Then, we propose in the next section to study acceptable level of PR bias estimation using a 3D simulator to obtain better positioning accuracy than the conventional algorithm like LS. This admissible region of inaccuracy will be defined theoretically in next section and validated in the last section using real GNSS data.

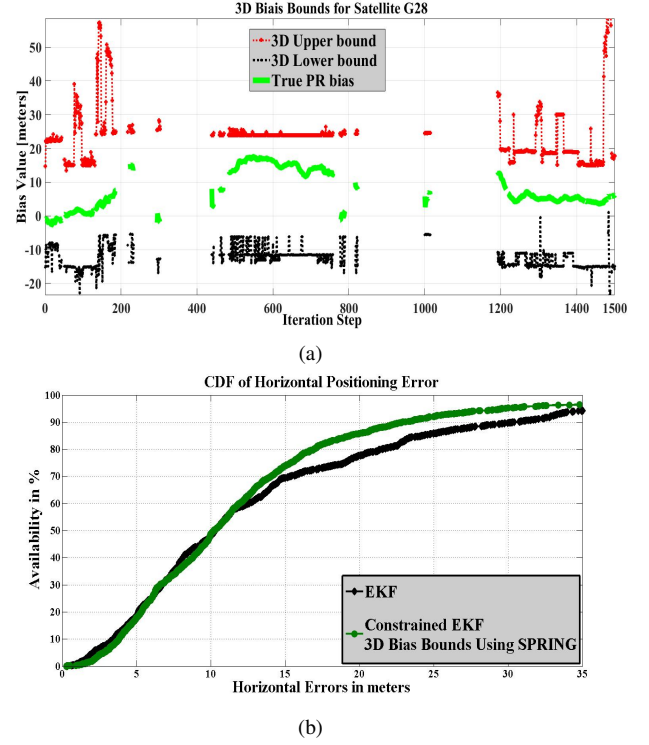


Fig. 7: Positioning performances using 3D bias bounds: 7(a) 3D Bias Bounds, 3D estimated bias at reference position and True bias for satellite PRN 28; 7(b) CDF of horizontal errors along the considered trajectory using 3D bias bounds estimation.

V. PERFORMANCES ENHANCEMENT BY GNSS PSEUDORANGES CORRECTION

A. Simulator Requirements for Performance Improvement

1) Requirement for Accuracy Improvement:

The fundamental question addressed in this sub-section is: how much accurate the PR bias estimation, by a 3D simulator or others tools, should be to ensure that the proposed CLS algorithm give better results in term of accuracy than the conventional LS. This amounts to find the maximum acceptable level of uncertainty on the PR bias prediction required to obtain a performance enhancement compared to conventional positioning algorithms such as least squares algorithm. The maximum acceptable level of inaccuracy in PR bias prediction to achieve better accuracy performance by PR correction compared to the conventional LS is defined by using the OMSE of the CLS estimator as:

$$OMSE[\hat{\mathbf{x}}_{CLS}] = \text{Tr}\{\mathbf{MSE}(\hat{\mathbf{x}}_{CLS})\} \leq OMSE[\hat{\mathbf{x}}_{LS}] = \text{Tr}\{\mathbf{MSE}(\hat{\mathbf{x}}_{LS})\}$$

In case of uncorrelated MP-NLOS bias \mathbf{b} , this leads to:

$$\begin{aligned} & \text{Tr}\{\mathbf{H}_b^+ E\{\delta\mathbf{b}\delta\mathbf{b}^T\}\mathbf{H}_b^+\} \leq \text{Tr}\{\mathbf{H}_0^+ E\{\mathbf{b}\mathbf{b}^T\}(\mathbf{H}_0^+)^T\} - \beta_{\mathbf{b}} \\ \Rightarrow & \sum_{k,i} [(\mathbf{H}_b^+)^T]_{k,i}^2 (E\{\delta\mathbf{b}\delta\mathbf{b}^T\})_i \leq \sum_{k,i} [(\mathbf{H}_0^+)^T]_{k,i}^2 (E\{\mathbf{b}\mathbf{b}^T\})_i - \beta_{\mathbf{b}} \end{aligned} \quad (24)$$

Proof: See Appendix B.

Where $\beta_{\mathbf{b}} = \text{Tr}\{(\mathbf{H}_0^T \mathbf{R}_b^{-1} \mathbf{H}_0)^{-1}\} - \text{Tr}\{(\mathbf{H}_0^T \mathbf{R}^{-1} \mathbf{H}_0)^{-1}\}$. In the case of only one faulty measurement in the ranging

measurement from one satellite j , i.e. \mathbf{b} contains only one non-zero value, this condition can be simplified as:

$$\sum_k [(\mathbf{H}_b^+)^+_{k,j}]^2 (E\{\delta\mathbf{b}\delta\mathbf{b}^T\})_j \leq \sum_k [(\mathbf{H}_0^+)^+_{k,j}]^2 (E\{\mathbf{b}\mathbf{b}^T\})_j - \beta_b$$

If we define the damping coefficient $\epsilon_j = \frac{\sum_k [(\mathbf{H}_0^+)^+_{k,j}]^2}{\sum_k [(\mathbf{H}_b^+)^+_{k,j}]^2}$,

then we have:

$$(E\{\delta\mathbf{b}\delta\mathbf{b}^T\})_j \leq \epsilon_j (E\{\mathbf{b}\mathbf{b}^T\})_j - (\beta_b / \sum_k [(\mathbf{H}_b^+)^+_{k,j}]^2) \quad (25)$$

This damping coefficient appears because we have augmented the noise covariance matrix \mathbf{R}_b using the PR bias prediction \mathbf{c} . If we haven't use this augmentation, i.e. $\mathbf{R}_b = \mathbf{R}$, then the damping coefficient ϵ_j will be equal to 1 and $\beta_b = 0$. Thus, the condition (25) became:

$$(E\{\delta\mathbf{b}\delta\mathbf{b}^T\})_j \leq (E\{\mathbf{b}\mathbf{b}^T\})_j \quad (26)$$

This condition means that the bias bound prediction error must have a lower variation than the true unknown PR bias variation to obtain better performance by correcting the PR measurement. The damping coefficient allows widening the admissible region of bias estimation inaccuracy since it is higher than 1, in general.

The condition (24) is a general condition that any positioning algorithm based on the PR measurements correction must verify to ensure lower estimation errors than conventional least squares algorithm without PR measurement correction. This condition defines the maximum acceptable level of uncertainty on the PR bias prediction in terms of positioning accuracy. Condition (24), obtained in the case of only one faulty ranging measurement, will be validated using true GNSS data in the last section of this article.

2) Accuracy Improvement indicator:

We can define the following positioning accuracy enhancement/degradation percentage obtained after PR measurements correction as:

$$\rho_{Accuracy} = \frac{OMSE[\hat{\mathbf{x}}_{LS}] - OMSE[\hat{\mathbf{x}}_{CLS}]}{OMSE[\hat{\mathbf{x}}_{LS}]} \quad (27)$$

$\rho_{Accuracy}$ reflects the accuracy enhancement by PR correction compared to LS algorithm. If we have a good bias prediction using 3D simulator, i.e. $\delta\mathbf{b}$ decrease, then $OMSE[\hat{\mathbf{x}}_{CLS}]$ will decrease and hence $\rho_{Accuracy}$ increase.

B. Requirement in case of Gaussian Bias Prediction Error

In this sub-section, we consider the particular case of a Gaussian PR bias prediction error $\delta\mathbf{b}$. We consider the case of only one faulty measurement in the ranging measurement obtained from satellite j . We suppose that the bias prediction error of the measurement from this satellite $\delta b = (\delta\mathbf{b})_j$ follows a Gaussian distribution $(\delta\mathbf{b})_j \sim \mathcal{N}(\mu, \sigma^2)$. Since the MSE matrix is diagonal, we have this relation between the Root Mean Square Error (RMSE) and the Overall Mean Square Error (OMSE): $RMSE = \sqrt{OMSE}$. The previous relation will be verified by simulations in the next section.

The OMSE and the RMSE are functions of the bias prediction errors as:

$$\begin{aligned} OMSE(\mu, \sigma) &= \text{Tr}\{(\mathbf{H}_0^T \mathbf{R}_b^{-1} \mathbf{H}_0)^{-1}\} + \sum_k [(\mathbf{H}_b^+)^+_{k,j}]^2 E\{\delta\mathbf{b}\delta\mathbf{b}^T\}_j \\ &= \text{Tr}\{(\mathbf{H}_0^T \mathbf{R}_b^{-1} \mathbf{H}_0)^{-1}\} + \sum_k [(\mathbf{H}_b^+)^+_{k,j}]^2 (\sigma^2 + \mu^2) \end{aligned} \quad (28a)$$

$$\begin{aligned} RMSE(\mu, \sigma) &= \sqrt{OMSE(\mu, \sigma)} \\ &= \sqrt{\text{Tr}\{(\mathbf{H}_0^T \mathbf{R}_b^{-1} \mathbf{H}_0)^{-1}\} + \sum_k [(\mathbf{H}_b^+)^+_{k,j}]^2 (\sigma^2 + \mu^2)} \end{aligned} \quad (28b)$$

Proof: See Appendix B.

In this case, the condition on the mean μ and the variance σ^2 of this bias estimation error on satellite j , i.e. $(\delta\mathbf{b})_j$, to obtain better positioning performance than the LS algorithm is as follows:

$$\begin{aligned} (E\{\delta\mathbf{b}\delta\mathbf{b}^T\})_j &\leq \epsilon_j (E\{\mathbf{b}\mathbf{b}^T\})_j - (\beta_b / \sum_k [(\mathbf{H}_b^+)^+_{k,j}]^2) \\ \Rightarrow (\sigma^2 + \mu^2) &\leq \epsilon_j (E\{\mathbf{b}\mathbf{b}^T\})_j - (\beta_b / \sum_k [(\mathbf{H}_b^+)^+_{k,j}]^2) \end{aligned} \quad (29)$$

It can be easily verified that if the error in the bias prediction $(\delta\mathbf{b})_j$ increase, i.e. μ and σ are high, $OMSE(\mu, \sigma)$ and $RMSE(\mu, \sigma)$ increase, meaning that the positioning accuracy decrease, i.e. $\rho_{Accuracy}$ decrease. Relations (28a), (28b) and (29) obtained in this particular case will be verified using real GNSS data in the next section.

VI. EXPERIMENTAL RESULTS

The purpose of this section is to investigate on the impact of PR bias estimation on the GNSS-based localization performance in term of positioning accuracy. Theoretical conditions have been established in the fourth section in (28a), (28b) and (29). Then, the aim of this section is to validate these conditions in a simplified case of one faulty ranging measurement. This study seeks to find the maximum acceptable level of uncertainty on the PR bias prediction required to obtain a performance enhancement compared to conventional positioning algorithms such as the conventional least squares. This maximum acceptable level of PR bias prediction uncertainty will define the minimum degree of realism that any 3D GNSS simulator must achieve to make the proposed method based on PR measurement correction more efficient than conventional methods.

The bias prediction error can be defined as: $\delta\mathbf{b} = \mathbf{b} - \mathbf{c}$. As this vector has N values corresponding to the received PR measurements, the sensibility analysis is difficult to be executed by varying these N values together. Since the MP/NLOS biases of different satellites are uncorrelated and without loss of generality, we have chosen to study the influence of the estimation of the bias satellite by satellite along the entire trajectory. Then, we start by correcting the PR measurements from all satellites using the true bias estimation using [33], except for one satellite, which is the satellite under study (PRN 28 in this case). We consider that we have only one unhealthy ranging measurement (from satellite PRN 28)

and we study the influence of the corresponding bias prediction error on the localization performance by measurement correction. To find the maximum acceptable level of bias prediction error required for performance enhancement, we introduce an artificial mean and variance such as the bias prediction error for one satellite vary according a Gaussian distribution meaning that:

$$(\delta \mathbf{b})_{\text{Satellite}=PRN28} \sim \mathcal{N}(\mu, \sigma^2); \quad (\delta \mathbf{b})_{\text{Satellite} \neq PRN28} = 0$$

The investigation on the influence of the bias prediction error on the proposed algorithms performance will be based on studying the variation of the mean, termed as shift also in this paper, and the variance of this Gaussian distribution on the localization performance. Performance indicators used are the position accuracy computed via the Root Mean Square Error and the Overall Mean Square Error:

$$OMSE = \sum_{i=1}^{Npoint} \frac{\|\mathbf{X}_{LS-Estimated}^i - \mathbf{X}_{reference}^i\|_2^2}{Npoint}$$

where $Npoint$ is the number of samples in the trajectory tested (the same trajectory as in the previous study in section 3 and represents in this case the number of Monte-Carlo iterations. Since the \mathbf{MSE} matrix is diagonal, we have this relation: $RMSE = \sqrt{OMSE}$ that will be verified by simulations. Finally, we suppose that $\mathbf{R}_b = \mathbf{R}$.

The following figure illustrates the RMSE and the OMSE variation depending on the mean and the standard deviation of the bias prediction error Gaussian distribution.

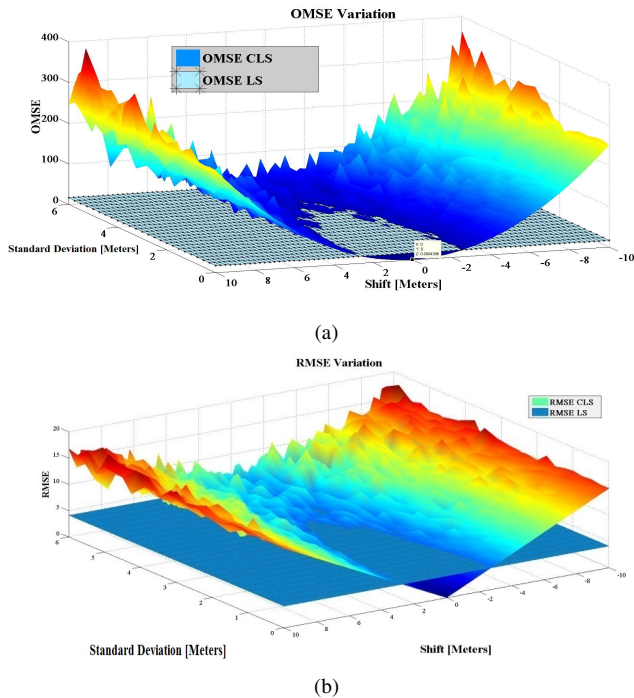


Fig. 8: Accuracy analysis for LS and CLS: 8(a) OMSE; 8(b) RMSE.

Constant curves, i.e. the flat curves in blue, correspond to the RMSE and the OMSE obtained using the conventional Least Squares. It is normal to get constant curves with LS in 8(a) and 8(b) since this estimator is computed without

bias correction and hence doesn't depends on the mean μ and the standard deviation σ of the bias correction term. The other variable curves in 8(a) and 8(b) correspond to the variation of the RMSE and the OMSE obtained using measurement correction. First, it can be easily seen that the RMSE variation correspond to the root of the OMSE variation. Second, both curves, i.e. the curves of RMSE and OMSE of both conventional LS and LS with PR measurement correction, follow the variation predicted using the theoretical study and summarized in (28a) and (28b). Both figures show that a bad bias prediction will lead to higher positioning errors by PR correction compared to the LS estimator.

The top view of the RMSE variation curve in Fig. 9 illustrates a region of acceptable bias prediction error defined as the region of bias prediction error allowing performance enhancement compared to conventional algorithms such as the conventional least squares in this case. Fig. 9 shows this region of maximum acceptable margin of error in bias prediction error using a 3D GNSS simulator, hence, the minimum degree of realism on 3D simulation, using SPRING simulator in this studied environment, necessary to ensure better positioning accuracy by measurement correction.

Equation (29) specifies the condition that this region of acceptable bias prediction error must verify. This equation describes a region of acceptable bias prediction error with a semi oval shape as shown in 9(b) which validates the condition (29). We can notice that we have a small and limited region of acceptable PR bias prediction error for this satellite and in this scenario which means that any tool that aim to predict the PR bias, such as a 3D GNSS simulator, must have a high level of realism and accuracy to successively estimate this bias and obtain better positioning performance than conventional algorithms.

We compare now the accuracy indicator depending on the error on PR bias prediction. The variation of the positioning accuracy enhancement/degradation percentage, expressed in (27), is shown in Fig. 10 versus the mean μ and the standard deviation σ of the bias correction term. Correcting PR bias will induce an accuracy enhancement compared to the conventional least squares when the error in the bias prediction is confined in a region of acceptable PR bias estimation error as shown in Fig. 9. However, this accuracy enhancement/degradation indicator is optimal when the predicted bias is following the variation of the true bias.

Finally, the PR measurement correction term must be as close as possible to the true ranging bias to obtain a positioning accuracy enhancement compared to conventional PVT estimators; if not this pseudorange measurement correction will lead to performance degradations.

VII. CONCLUSION

A considerable amount of literature has been published on the GNSS positioning in harsh environments. These studies aim generally to mitigate PR biases instead of their constructive use. This research sheds new lights on the constructive use of signals contaminated by MP and NLOS biases by bounding these erroneous PR measurements. The key strength of this

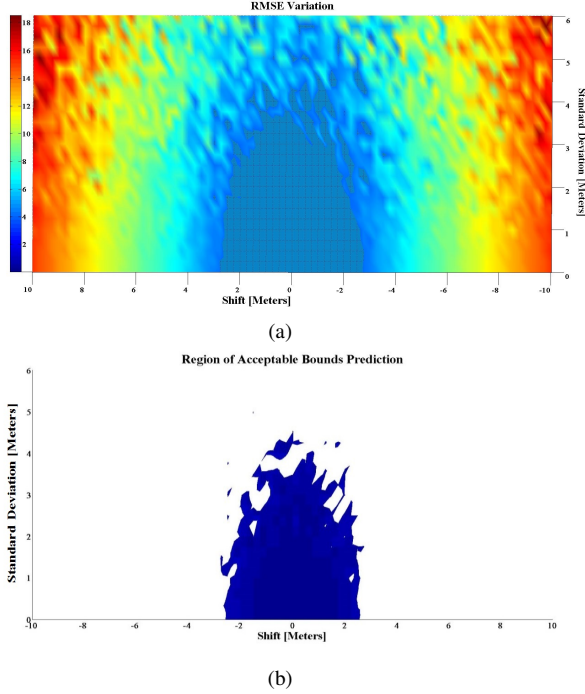


Fig. 9: Acceptable bias estimation error region: 9(a) RMSE variation for LS and CLS with the acceptable level of bias prediction error; 9(b) Top view of the acceptable bias estimation error region (consistent with (29)).

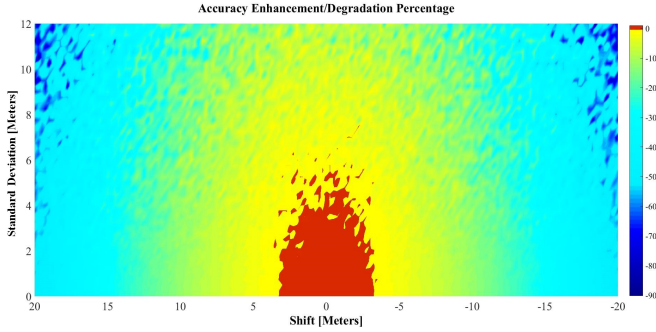


Fig. 10: Positioning accuracy enhancement/degradation percentage

study is its optimal effectiveness when the PR bias bounds are well predicted with respect to the true bias. Although the current study is based on one trajectory tested in an urban environment in Toulouse, the findings suggest that the proposed algorithm gives good positioning accuracy in case of predicted bias bounds following approximately the true bias variation.

Another aspect has been studied in sections 4 and 5, which is related to the question of how accurate the PR bias prediction should be to ensure that PR measurement correction will give better positioning accuracy than conventional positioning algorithms without measurement correction such as the conventional LS. This amounts to finding the maximum acceptable level of uncertainty on the PR bias prediction required to obtain a performance enhancement by PR measurements correction. This sensitivity analysis allows defining a maximum acceptable region of PR bias prediction error which is equivalent to defining a minimum degree of realism that any 3D simulator must achieve to ensure that PR

measurements correction will induce accuracy enhancement.

In this matter, it has been shown in this particular example of urban positioning that 3D GNSS Simulator SPRING achieves good degree of realism below the required level since PR measurements correction using this software gives better positioning accuracy than conventional algorithms. Furthermore, it is shown in [34] that the level of bias estimation uncertainty using the simulator SPRING is under the maximum allowed level. Hence, most of the time, the level of realism on bias prediction using this simulator allows PR bias correction and performance enhancement in these kinds of harsh environments. However, if diffraction and NLOS are present and accumulated and not accounted for in the simulation at a certain position or instant of time, the simulation result may be quite different from reality.

Further work could focus on enhancing the 3D city modeling and propagation simulation to reach the required level of realism, making the proposed method more and more effective. A natural progression of this work is to analyze the effectiveness of the proposed algorithm in other environments and with different 3D city models to make a general conclusion. This would be a fruitful area for further studies.

APPENDIX A: ML ESTIMATOR AND DERIVATION OF THE MSE OF THE ML AND LS ESTIMATORS

By definition, the maximum likelihood (ML) estimator is the estimator minimizing the likelihood function:

$$\hat{\mathbf{x}}_{ML} = \underset{\mathbf{x}}{\operatorname{argmin}} J(\mathbf{y}|\mathbf{x}, \mathbf{b})$$

The likelihood function can be expressed as:

$$\begin{aligned} J(\mathbf{y}|\mathbf{x}, \mathbf{b}) &= \|\mathbf{y} - \mathbf{H}_0\mathbf{x} - \mathbf{b}\|_{\mathbf{R}^{-1}}^2 \\ &= \|\Pi_{\mathbf{R}^{-1}}^{\mathbf{H}_0}(\mathbf{y} - \mathbf{H}_0\mathbf{x} - \mathbf{b})\|_{\mathbf{R}^{-1}}^2 + \|\Pi_{\mathbf{R}^{-1}}^{\mathbf{H}_0^\perp}(\mathbf{y} - \mathbf{H}_0\mathbf{x} - \mathbf{b})\|_{\mathbf{R}^{-1}}^2 \\ &= \|\Pi_{\mathbf{R}^{-1}}^{\mathbf{H}_0}(\mathbf{y} - \mathbf{b}) - \mathbf{H}_0\mathbf{x}\|_{\mathbf{R}^{-1}}^2 + \|\Pi_{\mathbf{R}^{-1}}^{\mathbf{H}_0^\perp}(\mathbf{y} - \mathbf{b})\|_{\mathbf{R}^{-1}}^2 \end{aligned}$$

This yields the following expression for the ML estimator:

$$\begin{aligned} \hat{\mathbf{x}}_{ML} &= \underset{\mathbf{x}}{\operatorname{argmin}} \|\Pi_{\mathbf{R}^{-1}}^{\mathbf{H}_0}(\mathbf{y} - \mathbf{b}) - \mathbf{H}_0\mathbf{x}\|_{\mathbf{R}^{-1}}^2 \\ &= \underset{\mathbf{x}}{\operatorname{argmin}} \|\mathbf{H}_0(\mathbf{H}_0^+(\mathbf{y} - \mathbf{b}) - \mathbf{x})\|_{\mathbf{R}^{-1}}^2 \end{aligned}$$

where $\mathbf{H}_0^+ = (\mathbf{H}_0^T \mathbf{R}^{-1} \mathbf{H}_0)^{-1} \mathbf{H}_0^T \mathbf{R}^{-1}$ is the pseudo-inverse of \mathbf{H}_0 weighted by the inverse of the measurements covariance matrix \mathbf{R} . This last expression gives the final expression of the ML estimator, given in (7) :

$$\hat{\mathbf{x}}_{ML} = \mathbf{H}_0^+(\mathbf{y} - \mathbf{b}) \iff \mathbf{H}_0 \hat{\mathbf{x}}_{ML} = \Pi_{\mathbf{R}^{-1}}^{\mathbf{H}_0}(\mathbf{y} - \mathbf{b})$$

The MSE of this ML estimator is defined as:

$$\begin{aligned} \mathbf{MSE}[\hat{\mathbf{x}}_{ML}] &= E[\delta \mathbf{x}_{ML} \delta \mathbf{x}_{ML}^T] = E[(\mathbf{H}_0^+ \mathbf{v})(\mathbf{H}_0^+ \mathbf{v})^T] \\ &= E[\mathbf{H}_0^+ \mathbf{v} \mathbf{v}^T (\mathbf{H}_0^+)^T] = \mathbf{H}_0^+ E[\mathbf{v} \mathbf{v}^T] (\mathbf{H}_0^+)^T \end{aligned}$$

As $E\{\mathbf{v} \mathbf{v}^T\} = \mathbf{R}$, then this yields:

$$\begin{aligned} \mathbf{MSE}[\hat{\mathbf{x}}_{ML}] &= \mathbf{H}_0^+ \mathbf{R} (\mathbf{H}_0^+)^T \\ &= (\mathbf{H}_0^T \mathbf{R}^{-1} \mathbf{H}_0)^{-1} \mathbf{H}_0^T \mathbf{R}^{-1} \mathbf{R} \mathbf{R}^{-1} \mathbf{H}_0 (\mathbf{H}_0^T \mathbf{R}^{-1} \mathbf{H}_0)^{-1} \\ &= (\mathbf{H}_0^T \mathbf{R}^{-1} \mathbf{H}_0)^{-1} \end{aligned}$$

This proves relation (9). Using the same derivation, we can prove the MSE derivation of the LS estimator given in (12):

$$\begin{aligned} \text{MSE}[\hat{\mathbf{x}}_{LS}] &= E[\delta\mathbf{x}_{LS}\delta\mathbf{x}_{LS}^T] = E[(\mathbf{H}_0^+(\mathbf{v} + \mathbf{b}))(\mathbf{H}_0^+(\mathbf{v} + \mathbf{b}))^T] \\ &= E[\mathbf{H}_0^+\mathbf{v}\mathbf{v}^T(\mathbf{H}_0^+)^T] + E[\mathbf{H}_0^+\mathbf{b}\mathbf{b}^T(\mathbf{H}_0^+)^T] \\ &= (\mathbf{H}_0^T\mathbf{R}^{-1}\mathbf{H}_0)^{-1} + \mathbf{H}_0^+ E[\mathbf{b}\mathbf{b}^T](\mathbf{H}_0^+)^T \end{aligned}$$

APPENDIX B: PR BIAS PREDICTION UNCERTAINTY

Proof of Relation (24)

We start from the accuracy requirement from V-A1:

$$\text{OMSE}[\hat{\mathbf{x}}_{CLS}] \leq \text{OMSE}[\hat{\mathbf{x}}_{LS}]$$

The expressions of the OMSE of CLS and LS estimators are given in (18) and (13) and are recalled below:

$$\begin{cases} \text{OMSE}[\hat{\mathbf{x}}_{LS}] &= \text{Tr}\{(\mathbf{H}_0^T\mathbf{R}^{-1}\mathbf{H}_0)^{-1}\} + \text{Tr}\{\mathbf{H}_0^+ E\{\mathbf{b}\mathbf{b}^T\}(\mathbf{H}_0^+)^T\} \\ \text{OMSE}[\hat{\mathbf{x}}_{CLS}] &= \text{Tr}\{(\mathbf{H}_0^T\mathbf{R}_b^{-1}\mathbf{H}_0)^{-1}\} + \text{Tr}\{\mathbf{H}_b^+ E\{\delta\mathbf{b}\delta\mathbf{b}^T\}(\mathbf{H}_b^+)^T\} \end{cases}$$

If we note the following term $\beta_b = \text{Tr}\{(\mathbf{H}_0^T\mathbf{R}_b^{-1}\mathbf{H}_0)^{-1}\} - \text{Tr}\{(\mathbf{H}_0^T\mathbf{R}^{-1}\mathbf{H}_0)^{-1}\}$, the accuracy requirement expressed at the beginning of this appendix can be written as:

$$\text{Tr}\{\mathbf{H}_b^+ E\{\delta\mathbf{b}\delta\mathbf{b}^T\}\mathbf{H}_b^+\} \leq \text{Tr}\{\mathbf{H}_0^+ E\{\mathbf{b}\mathbf{b}^T\}(\mathbf{H}_0^+)^T\} - \beta_b$$

Now, the OMSE of both LS and CLS estimators, can be expressed using the trace operator proprieties as:

$$\begin{cases} \text{OMSE}[\hat{\mathbf{x}}_{LS}] &= \sum_{k,i} [(\mathbf{H}_0^+)^T]_{k,i}^2 E\{\mathbf{b}\mathbf{b}^T\}_{i,i} + \text{Tr}\{(\mathbf{H}_0^T\mathbf{R}^{-1}\mathbf{H}_0)^{-1}\} \\ \text{OMSE}[\hat{\mathbf{x}}_{CLS}] &= \sum_{k,i} [(\mathbf{H}_b^+)^T]_{k,i}^2 E\{\delta\mathbf{b}\delta\mathbf{b}^T\}_{i,i} + \text{Tr}\{(\mathbf{H}_0^T\mathbf{R}_b^{-1}\mathbf{H}_0)^{-1}\} \end{cases}$$

Proof of Relation (28a)

The OMSE of the CLS estimator is given by:

$$\text{OMSE}[\hat{\mathbf{x}}_{CLS}] = \sum_{k,i} [(\mathbf{H}_b^+)^T]_{k,i}^2 E\{\delta\mathbf{b}\delta\mathbf{b}^T\}_{i,i} + \text{Tr}\{(\mathbf{H}_0^T\mathbf{R}_b^{-1}\mathbf{H}_0)^{-1}\}$$

In case of only one ranging measurement error from satellite j and when correcting the ranging errors from all received satellites except satellite j , i.e. $(\delta\mathbf{b})_j \neq 0$ and $(\delta\mathbf{b})_{i \neq j} = 0$, the sum present in the previous expression can be simplified:

$$\sum_{k,i} [(\mathbf{H}_b^+)^T]_{k,i}^2 E\{\delta\mathbf{b}\delta\mathbf{b}^T\}_{i,i} = \sum_k [(\mathbf{H}_b^+)^T]_{k,j}^2 E\{\delta\mathbf{b}\delta\mathbf{b}^T\}_j$$

As $(\delta\mathbf{b})_j \sim \mathcal{N}(\mu, \sigma^2)$, then $E\{\delta\mathbf{b}\delta\mathbf{b}^T\}_j = \sigma^2 + \mu^2$, which proves relation (28a).

REFERENCES

- [1] GSA, "GNSS Market Report Issue 5," GSA, Tech. Rep., May, 2017, doi:10.2878/0426.
- [2] L. Wang, P. D. Groves, and M. K. Ziebart, "GNSS Shadow Matching: Improving Urban Positioning Accuracy Using a 3D City Model with Optimized Visibility Prediction Scoring," in *Proc. of ION GNSS 2012*.
- [3] P. D. Groves, Z. Jiang, L. Wang, and M. K. Ziebart, "Intelligent Urban Positioning using Multi-Constellation GNSS with 3D Mapping and NLOS Signal Detection," in *Proc. of ION GNSS 2012*, no. 458 - 472.
- [4] P. Groves, "Multipath vs. NLOS signals. How Does Non-Line-of-Sight Reception Differ from Multipath Interference," *Inside GNSS 2013*.
- [5] A. J. Van Dierendonck, P. Fenton, and T. Ford, "Theory and Performance of Narrow Correlator Spacing in a GPS Receiver," *Navigation 1992*.
- [6] M. S. Braasch, "Performance comparison of multipath mitigating receiver architectures," in *Proc. IEEE Aerospace Conference*, vol. 3, 2001.
- [7] M. S. Braasch and R. J. Landry, "Multipath Mitigation Techniques using Maximum-Likelihood Principles," *Inside GNSS 2008*.
- [8] G. A. McGraw and M. S. Braasch, "GNSS Multipath Mitigation Using Gated and High Resolution Correlator Concepts."
- [9] L. Garin, F. van Diggelen, and J.-M. Rousseau, "Strobe & Edge Correlator Multipath Mitigation for Code," in *Proceedings of ION GPS 1996, Kansas City, MO*, September 1996, pp. 657-664.
- [10] R. Ercek, P. De Doncker, and F. Grenez, "Statistical determination of the PR error due to NLOS-Multipath in urban canyons," in *Proc. of ION GNSS 2006*.
- [11] I. Givenc and C. C. Chong, "A Survey on TOA Based Wireless Localization and NLOS Mitigation Techniques," *IEEE Communications Surveys Tutorials*, vol. 11, no. 3, pp. 107-124, rd 2009.
- [12] P. D. Groves, Z. Jiang, B. Skelton, P. A. Cross, L. Lau, Y. Adane, and I. Kale, "Novel multipath mitigation methods using a dual-polarization antenna." Institute of Navigation, 2010.
- [13] J. Marais, M. Berbineau, and M. Heddebaut, "Land mobile gnss availability and multipath evaluation tool," *IEEE Transactions on Vehicular Technology*, vol. 54, no. 5, pp. 1697-1704, Sept 2005.
- [14] P. D. Groves and Z. Jiang, "Height Aiding, C/N0 Weighting and Consistency Checking for GNSS NLOS and Multipath Mitigation in Urban Areas," *Journal of Navigation*, pp. 653-659, 2013.
- [15] S. Peyraud, D. Bétaille, S. Renault, M. Ortiz, F. Mougél, D. Meizel, and F. Peyret, "About non-line-of-sight satellite detection and exclusion in a 3D map-aided localization algorithm," *Sensors*, vol. 13, no. 1.
- [16] J. Marais, S. Tay, A. Flancquart, and C. Meurie, "Weighting with the pre-knowledge of GNSS signal state of reception in urban areas," in *European Navigation Conference 2015*, 2015, p. 7p.
- [17] K. Fallahi, C.-T. Cheng, and M. Fattouche, "Robust positioning systems in the presence of outliers under weak GPS signal conditions," *IEEE Systems Journal*, vol. 6, no. 3, pp. 401-413, 2012.
- [18] T. Perala, *Robust Kalman-type filtering in positioning applications*. INTECH Open Access Publisher, 2010.
- [19] P. Groves, *Principles of GNSS, Inertial, and Multisensor Integrated Navigation Systems, Second Edition*. Artech House, 2013.
- [20] A. Rabaoui, N. Viandier, E. Duflos, J. Marais, and P. Vanheeghe, "Dirichlet Process Mixtures for Density Estimation in Dynamic Non-linear Modeling: Application to GPS Positioning in Urban Canyons," *IEEE Transactions on Signal Processing*, vol. 60, no. 4, 2012.
- [21] M. Spangenberg, J. Y. Tourneret, V. Calmettes, and G. Duchateau, "Detection of variance changes and mean value jumps in measurement noise for multipath mitigation in urban navigation," in *Proc. of Asilomar Conference on Signals, Systems and Computers 2008*.
- [22] A. Bourdeau, M. Sahnoudi, and J.-Y. Tourneret, "Constructive use of GNSS NLOS-multipath: Augmenting the navigation Kalman filter with a 3D model of the environment," in *Proc. of FUSION 2012*. IEEE.
- [23] —, "Tight Integration of GNSS and a 3D City Model for Robust Positioning in Urban Canyons," in *Proceedings of ION GNSS 2012, Nashville, TN*, September, 2012, pp. 1263-1269.
- [24] K. A. B. Ahmad, M. Sahnoudi, C. Macabiau, A. Bourdeau, and G. Moura, "Reliable gnss positioning in mixed los/nlos environments using a 3d model," in *ENC 2013, European Navigation Conference*, 2013, pp. pp-xxxx.
- [25] M. Adjrard and P. D. Groves, "Intelligent Urban Positioning using Shadow Matching and GNSS Ranging aided by 3D Mapping," in *Proceedings of ION GNSS+*, Portland, September 2016.
- [26] R. Kumar and M. G. Petovello, "A novel GNSS positioning technique for improved accuracy in urban canyon scenarios using 3D city model," in *Proc. of ION GNSS+ 2014, Tampa, FL, USA*, vol. 812.
- [27] T. Suzuki and N. Kubo, "Correcting GNSS multipath errors using a 3D surface model and particle filter," *Proc. ION GNSS+ 2013*.
- [28] S. Miura, S. Hisaka, and S. Kamijo, "GPS multipath detection and rectification using 3D maps," in *Proc. of IEEE ITSC 2013*.
- [29] D. Bétaille, F. Peyret, M. Ortiz, S. Miquel, and L. Fontenay, "A new modeling based on urban trenches to improve GNSS positioning quality of service in cities," *IEEE Intelligent Transportation Systems Magazine*.
- [30] D. Bétaille, F. Peyret, M. Ortiz, S. Miquel, and F. Godan, "Improving accuracy and integrity with a probabilistic Urban Trench modeling," *Navigation*, vol. 63, no. 3, pp. 283-294, 2016.
- [31] S. M. Kay, *Fundamentals of statistical signal processing, volume I: estimation theory*. Prentice Hall, 1993.
- [32] N. Kbayer, M. Sahnoudi, and E. Chaumette, "Robust GNSS Navigation in Urban Environments by Bounding NLOS Bias of GNSS Pseudoranges Using a 3D City Model," in *Proceedings of ION GNSS+ 2015*.
- [33] T. Iwase, N. Suzuki, and Y. Watanabe, "Estimation and exclusion of multipath range error for robust positioning," *GPS solutions 2013*.
- [34] N. Kbayer and M. Sahnoudi, "Constructive Use of MP/NLOS bias of GNSS Pseudoranges: Performance Analysis by Type of Environment," in *Proc. of ION ITM 2017*.



Nabil Kbayer is a PhD student at the French Institute of Aeronautics and Space (ISAE-SUPAERO) and at TésA laboratory, University of Toulouse, France. He received his engineer degree in signal processing from the french institute of Aeronautics and Space *Ecole Nationale Supérieure d'Ingénieurs de Constructions Aéronautiques* (ISAE-ENSICA) in 2014. His research interests include signal processing for positioning in challenging environments, multipath and NLOS mitigation and constructive use for cognitive navigation.



Mohamed Sahnoudi received a PhD in signal processing and communications systems from Paris-Sud Orsay University, France, in collaboration with Telecom Paris in 2004. From 2005 to 2007, he was a post-doctoral researcher fellow on GPS Signal Processing and Navigation at Villanova University, PA, USA. In august 2007, he joined the ETS school of engineering at Montreal, Canada, to lead the research team of precise positioning (RTK and PPP). In 2009, he became an Associate Professor at ISAE-SUPAERO, University of Toulouse, France.

Currently his research interests focus on all aspects of signal processing for navigation in harsh environment, weak GNSS signals acquisition and tracking, multi-frequency and multi-GNSS receivers, multipath mitigation and constructive use and multi-sensor fusion for robust navigation.